Ultrasonic Speed of Sound and Derived Thermodynamic Properties of Liquid 1,1,1,2,3,3,3-Heptafluoropropane (HFC227ea) from 248 K to 333 K and Pressures up to 65 MPa

P. F. Pires, J. M. S. S. Esperança, and H. J. R. Guedes*

Departamento de Química, Centro de Química Fina e Biotecnologia, Faculdade de Ciências e Tecnologia, Universidade Nova de Lisboa, 2825−114 Caparica, Portugal

This work reports experimental data of the speed of sound in liquid 1,1,1,2,3,3,3-heptafluoropropane (HFC227ea) from 248 K to 333 K and pressures up to 65 MPa, measured with a pulse−echo method. The results are fitted with a rational approximant. Derived thermodynamic properties are calculated, combining our experimental data with density and isobaric heat capacity values published by other authors. The results were compared with the data available in the literature.

Introduction

The fluorinated propanes have recently been pointed out as promising alternatives to the chlorofluorocarbons used in the refrigeration industry (Weber and Defibaugh, 1996). 1,1,1,2,3,3,3-heptafluoropropane, commercially designated as HFC227ea, is one of the candidates and there are very few property measurements reported in the literature. Measurements include calorimetric data (Wirbser et al., 1992), density (Klomfar et al., 1994), and vapor pressure (Tuerk et al., 1994). The speed of sound, u, is a thermodynamic property that can be experimentally determined with great accuracy over a large range of temperature and pressure conditions, both in the liquid and gas phases. Since u can be related to the first pressure partial derivative of the density, high accuracy speed of sound data can be used to enhance, by an order of magnitude, the development of equations of state. Also, it is very useful as a source of information to compute the values of other thermodynamic properties difficult to obtain at extreme experimental conditions, such as calorimetric data at high pressures. In the present work, we have measured the ultrasonic speed of sound of HFC227ea in the liquid phase, with an apparatus designed to operate at elevated pressures. This apparatus has already been tested, and results reported for two other alternative refrigerants (Pires and Guedes, 1999a, Pires and Guedes, 1999b). The experimental data were fitted and used together with density and isobaric heat capacity data from other authors (Wirbser et al., 1992, Klomfar et al., 1994), to calculate, through an integration method (Sun et al., 1988), several thermodynamic properties such as the isentropic and isothermal compressibilities, β_S and β_T, the isobaric thermal expansion coefficient, α_p, the thermal pressure coefficient, γ_v, the isentalpic Joule−Thomson coefficient, μ_{JT}, isobaric and isochoric heat capacities, C_p, C_v, and enthalpy and entropy variations, relative to a reference state.

Experimental Section

The speed of sound of liquid HFC227ea was measured with an apparatus designed for high pressures, with an acoustic cell placed inside a stainless steel container, using a method previously described (Pires and Guedes, 1999a), i.e., the apparatus was operated with a pulse−echo method at a frequency of 1 MHz. The cell calibration was performed by measuring the speed of sound of pure CCl_4 at 10 MPa and 298.15 K, and comparing the obtained value with data reported in the literature (Kyohara et al., 1978, Lainez et al., 1987). To cover the complete experimental temperature and pressure ranges, the calibration was expanded by the use of the thermal and pressure behavior of the pure copper spacers (99.99+% purity) (*Metals Handbook*, 1979; White and Roberts, 1980).

The steel container and the acoustic cell were thermostated inside a Dewar vessel within the temperature range from $T = 248$ K to $T = 333$ K, with a control system based on a two-stage cascaded thermostatic baths. The long-term stability of the complete system was within ±0.02 K in the whole range and the temperature measurements were taken with a four-wire platinum resistance thermometer previously calibrated to an uncertainty of ±0.01 K, on ITS 90 scale.

Pressure measurements were performed in two separate ranges with a Setra Systems Inc. pressure transducer (from vapor pressure to 35 MPa) and a Digibar transducer (up to 65 MPa). The pressure sensors were calibrated against a dead weight gauge with an uncertainty of ±0.025 MPa in the lower range and ±0.2 MPa in the higher range.

When all of the the error sources are taken into account, the accuracy of the speed of sound measurements is estimated to be better than ±0.3 m s^{-1}. Several measurements were repeated at the same pressure and temperature conditions, allowing us to estimate a precision of ±0.1 m s^{-1}.

The HFC227ea used in the experimental work was supplied by Solvay Fluor und Derivate GmbH, with a stated purity of 0.9998 mass fraction. The sample was further dried with molecular sieves and three times degassed by condensation with liquid nitrogen, followed by a flush out.

Results and Discussion

The apparatus was used to take a total of 289 experimental speed of sound measurements of the alternative refrigerant HFC227ea, within the referred temperature

* To whom correspondence should be addressed. E-mail: h.guedes@dq.fct.unl.pt.

10.1021/je9902950 CCC: $19.00
Published on Web 04/26/2000

Table 1. Experimental Data of the Speed of Sound *u* of HFC227ea at Temperatures from *T* = 248 K to *T* = 333 K and Pressures *p* up to 65 MPa

p / MPa	*u* / m s^{-1}	*p* / MPa	*u* / m s^{-1}	*p* / MPa	*u* / m s^{-1}	*p* / MPa	*u* / m s^{-1}	*p* / MPa	*u* / m s^{-1}	*p* / MPa	*u* / m s^{-1}
					T = 248.08 K						
0.42	619.85	1.00	624.08	5.00	650.53	10.00	680.90	30.00	781.30	50.03	861.16
0.43	619.96	2.00	630.68	6.00	656.80	12.50	695.13	35.05	802.78	54.99	879.00
0.44	620.05	3.00	637.57	7.00	663.14	15.00	708.76	40.01	822.99	60.05	896.66
0.44	620.01	4.00	643.90	8.00	669.03	20.00	734.40	44.97	842.76	65.01	913.22
0.50	620.47	5.00	650.51	9.00	675.10	25.00	758.69	44.97	842.53		
					T = 253.21 K						
0.41	598.56	1.00	602.87	7.00	643.44	12.50	676.50	40.01	807.43	54.99	864.43
0.41	598.54	2.00	610.00	8.00	649.77	15.00	690.61	44.97	827.00	60.05	882.13
0.50	599.14	3.00	617.01	9.00	655.82	20.00	717.01	50.03	846.22	65.01	898.64
1.00	602.37	4.00	623.90	10.00	661.87	35.05	786.97				
					T = 263.20 K						
0.41	557.12	3.00	577.47	10.00	625.98	30.00	734.30	60.05	855.64	65.01	872.77
0.41	557.12	4.00	584.82	12.50	641.36	35.05	757.50	60.05	855.64	65.01	872.45
0.50	557.80	5.00	592.15	15.00	656.22	40.01	778.90	65.01	872.54	65.01	872.88
1.00	561.86	6.00	599.23	20.00	684.08	50.03	818.91				
2.00	569.76	9.00	619.41	25.00	710.20	54.99	837.63				
					T = 273.19 K						
0.40	515.95	1.00	521.33	7.00	596.59	12.50	607.45	35.05	728.86	54.99	811.38
0.40	515.96	2.00	529.97	8.00	576.84	15.00	623.22	40.01	751.12	60.05	830.19
0.40	515.97	3.00	538.29	9.00	583.95	20.00	652.49	44.97	771.82	65.01	847.80
0.50	516.75	4.00	546.41	10.00	590.91	25.00	679.69	50.03	792.19		
					T = 283.19 K						
0.39	475.31	1.00	481.45	6.00	525.97	12.50	574.86	30.00	677.24	54.99	787.59
0.39	475.38	2.00	491.03	7.00	534.15	15.00	591.49	35.05	702.58	60.05	806.01
0.39	475.38	3.00	500.25	8.00	541.91	20.00	622.31	40.01	725.12	65.01	823.72
0.39	475.35	4.00	509.17	9.00	549.68	25.00	650.97	44.97	746.30		
0.50	476.38	5.00	517.87	10.00	557.10	30.00	677.14	50.03	767.52		
					T = 293.17 K						
0.44	434.57	2.00	451.66	8.00	507.76	12.50	542.88	25.00	623.16	40.01	699.66
0.44	434.61	3.00	461.98	9.00	516.04	15.00	560.59	25.00	623.01	44.97	721.63
0.44	434.63	4.00	471.90	9.00	515.99	15.00	560.63	25.00	622.98	50.03	743.02
0.50	435.30	5.00	481.44	9.00	515.97	15.00	560.70	25.00	623.16	54.99	763.49
1.00	440.96	6.00	490.47	10.00	523.91	20.00	593.36	30.00	650.26	60.05	782.93
1.50	446.30	7.00	499.30	10.00	523.89	25.00	622.94	34.95	675.43	65.01	801.36
					T = 303.11 K						
0.56	394.88	2.00	412.69	7.00	465.31	15.00	531.01	40.01	675.71	54.99	741.10
0.56	394.89	3.00	424.30	8.00	474.52	20.00	565.47	44.97	698.35	60.05	761.06
0.57	394.91	4.00	435.28	9.00	483.41	25.00	596.44	50.03	720.59	65.01	780.12
0.57	394.92	5.00	445.80	10.00	491.91	30.00	624.65				
1.00	400.42	6.00	455.68	12.50	512.15	35.05	651.40				
					T = 313.13 K						
0.74	354.35	0.76	354.52	5.00	409.92	10.00	460.31	30.00	600.11	54.99	720.26
0.74	354.39	1.00	358.22	6.00	420.96	12.50	482.07	35.05	627.39	60.05	740.14
0.76	354.52	2.00	372.40	7.00	431.43	15.00	502.07	40.01	652.31	65.01	758.94
0.76	354.56	3.00	385.67	8.00	441.54	20.00	538.24	44.97	675.69		
0.76	354.59	4.00	398.09	9.00	451.20	25.00	570.64	50.03	698.10		
					T = 323.12 K						
0.96	313.50	3.00	346.99	9.00	419.90	20.00	512.35	50.03	677.79	65.01	739.71
0.96	313.50	4.00	361.31	10.00	429.78	25.00	545.95	54.99	699.54		
1.00	314.28	5.00	374.58	12.50	453.04	40.01	631.01	60.05	720.63		
2.00	331.59	8.00	409.45	15.00	474.27	44.97	655.03	60.05	720.23		
					T = 333.11 K						
1.21	271.73	3.00	307.39	9.00	389.34	20.00	487.59	50.03	657.38	60.05	701.13
1.21	271.78	4.00	323.96	10.00	400.15	25.00	522.70	54.99	679.72	65.01	720.77
1.49	280.28	5.00	339.19	12.50	425.16	40.01	609.76				
2.00	288.59	8.00	377.92	15.00	447.60	44.97	634.21				

and pressure ranges. These data are shown in Table 1. The measurements were performed and organized as isotherms, within a total of 10, and are plotted in Figure 1. The consistency of the individual isotherms was tested by fitting each one with

$$u = \sum_{i=0}^{2} A_i [\ln(p - B_i)]^i \qquad (1)$$

The standard deviations of the fits are smaller than 0.16 m s^{-1}, which indicates the high accuracy of the measurements.

This type of apparatus allows the direct measurement of the saturated liquid (orthobaric) speed of sound, u_σ, only above room temperature, which is about 295 K in our laboratory. To estimate the orthobaric speed of sound at the six lower temperature isotherms, eq 1 was also used to extrapolate them to the vapor pressure, p_σ (Tuerk et al., 1994). The estimated values are represented in Table 2, together with the directly measured values. The orthobaric speed of sound data were fitted to

$$u_\sigma = \sum_{i=0}^{4} A_i \left[\ln\left(\frac{T}{T_c}\right)\right]^i \qquad (2)$$

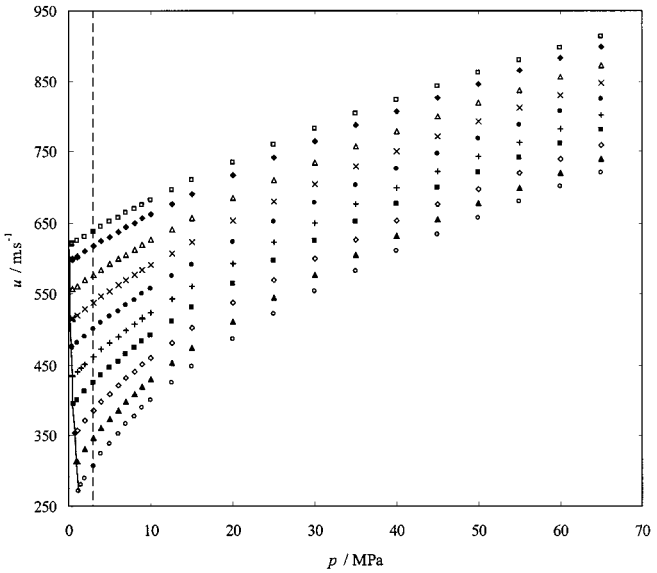

Figure 1. Plot of the experimental speed of sound u of HFC227ea: □, 248.08 K; ◆, 253.21 K; △, 263.20 K; ×, 273.19 K; ●, 283.19 K; +, 293.17 K; ■, 303.11 K; ◇, 313.13 K; ▲, 323.12 K; ○, 333.11 K; —, saturation; – – –, critical pressure.

Table 2. Orthobaric Speed of Sound of HFC227ea

T / K	p_σ / MPa	u_σ[a] / m s^{-1}	T / K	p_σ / MPa	u_σ[a] / m s^{-1}
248.08	0.069	617.41*	293.17	0.390	434.00*
253.21	0.087	596.07*	303.11	0.529	394.39
263.20	0.133	554.85*	313.13	0.702	353.71
273.19	0.197	513.38*	323.12	0.915	312.71
283.19	0.281	474.24*	333.11	1.174	271.32

[a] The asterisks (*) indicate extrapolated values.

Table 3. Coefficients of the Fit of u_σ to Eq 2

i	A_i
0	8.598E+01
1	−1.757E+03
2	−1.823E+03
3	−1.915E+03
4	−6.134E+02

(critical data $T_c = 375.05$ K and $p_c = 2.952$ MPa were taken from Klomfar et al., 1994) with the coefficients of Table 3. The standard deviation of the fit was ±0.4 m s^{-1}.

Finally, the whole set of speed of sound data was fitted to

$$u = \frac{\sum_{i=1}^{2}\sum_{j=0}^{2} A_{ij} p^i T^j}{\sum_{k=0}^{2}\sum_{l=0}^{2} B_{kl} p^k T^l} \qquad (3)$$

with the coefficients shown in Table 4, and a standard deviation of ±0.5 m s^{-1}. The percentage deviations between the experimental data and the fit are plotted in Figure 2, as a function of temperature.

As far as the authors are aware, there are no other speed of sound data to which the present work can be compared.

Derived Thermodynamic Properties

The speed of sound, u, is directly related to the pressure derivative of the density, ρ, through eq 4, in which the subscript S denotes the condition of constant entropy.

Table 4. Coefficients of the Fit of the Experimental Speed of Sound Data to Eq 3

A_{ij}	J		
i	0	1	2
0	1.842227E+03	−9.249117E+00	1.146473E−02
1	2.882827E+01	−4.687269E−02	−4.928242E−05
2	−1.224327E−01	1.455166E−03	−1.826586E−06
B_{kl}	L		
k	0	1	2
0	1.000000E+00	−1.749825E−03	−2.520361E−06
1	1.003639E−02	6.763951E−05	−1.413580E−07
2	−1.662420E−04	1.293750E−06	−1.433245E−09

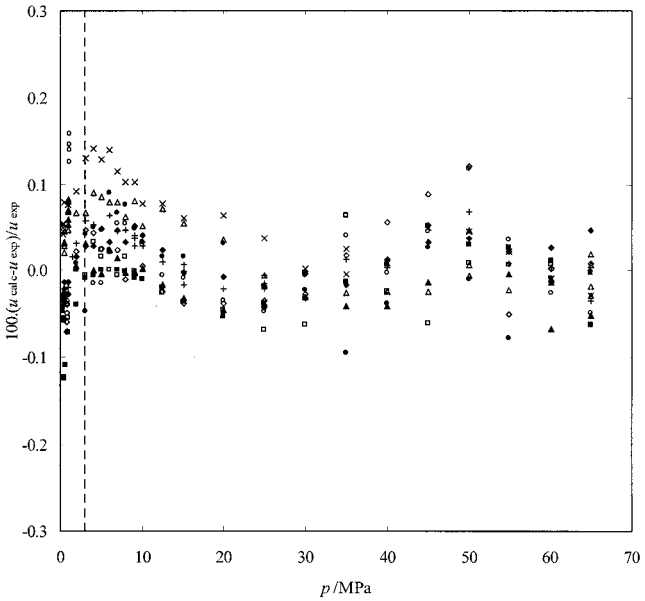

Figure 2. Plot of the percentage deviations of the experimental speed of sound (u_{exp}) to eq 3 (u_{calc}): □, 248.08 K; ◆, 253.21 K; △, 263.20 K; ×, 273.19 K; ●, 283.19 K; +, 293.17 K; ■, 303.11 K; ◇, 313.13 K; ▲, 323.12 K; ○, 333.11 K; —, saturation; – – –, critical pressure.

$$\left(\frac{\partial \rho}{\partial p}\right)_S = \frac{1}{u^2} \qquad (4)$$

This derivative is related to the isothermal pressure derivative and the isobaric temperature derivative of the density through eq 5, where C_p is the specific heat capacity at constant pressure.

$$\left(\frac{\partial \rho}{\partial p}\right)_S = \left(\frac{\partial \rho}{\partial p}\right)_T - \frac{T}{\rho^2 C_p}\left(\frac{\partial \rho}{\partial p}\right)_p^2 \qquad (5)$$

Rearranging the last equation and combining it with eq 4 creates eq 6, which also incorporates the definition of the thermal expansion coefficient, α_p:

$$\left(\frac{\partial \rho}{\partial p}\right)_T = \frac{1}{u^2} + \frac{T}{C_p}\alpha_p^2 \qquad (6)$$

$$\alpha_p = -\frac{1}{\rho}\left(\frac{\partial \rho}{\partial T}\right)_p \qquad (7)$$

It can also be shown that the pressure partial derivative of the isobaric heat capacity can calculated with eq 8:

$$\left(\frac{\partial C_p}{\partial p}\right)_T = -\frac{T}{\rho}\cdot\left[\alpha_p^2 + \left(\frac{\partial \alpha_p}{\partial T}\right)_p\right] \qquad (8)$$

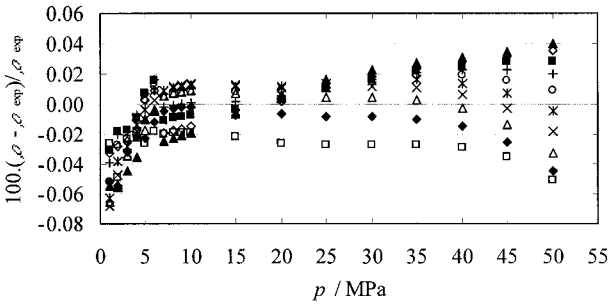

Figure 3. Percentage deviations between our results, ρ, and the fit of the literature experimental data, ρ_{exp} (Klomfar et al., 1994): □, 270 K; ◆, 275 K; △, 280 K; ×, 285 K; ∗, 290 K; ○, 295 K; +, 300 K; ■, 305 K; ◇, 310 K; ▲, 315.

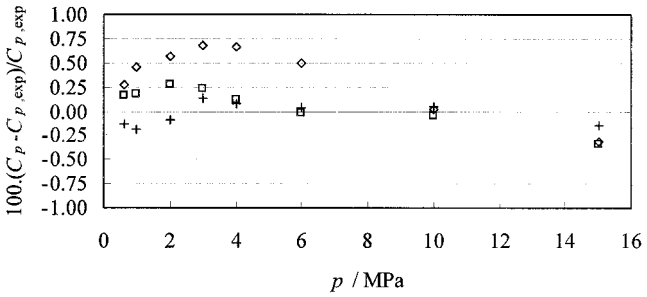

Figure 4. Percentage deviations between the integration heat capacity results, C_p, and the data from the literature, $C_{p,exp}$ (Wirbser et al., 1992): ◇, 273.15 K; □, 288.15 K; +, 303.15 K.

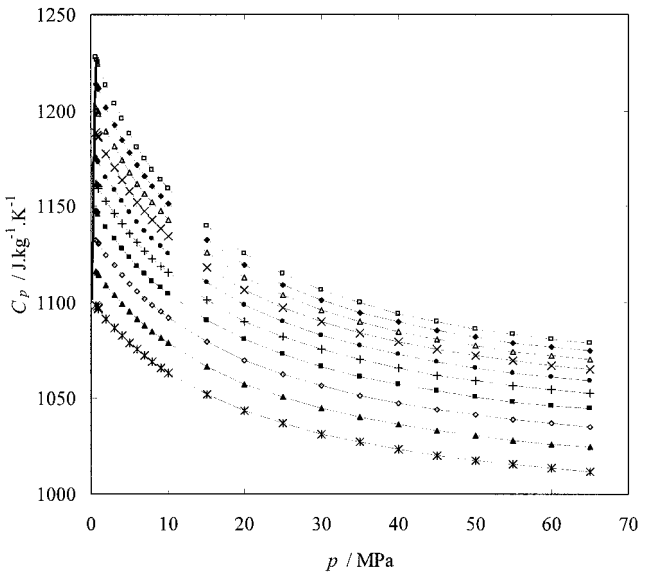

Figure 5. (p,C_p,T) surface: −∗−, 270 K; −▲−, 275 K; −◇−, 280 K; −■−, 285 K; −+−, 290 K; ●, 295 K; −×−, 300 K; −△−, 305 K; −◆−, 310 K; −□−, 315 K; —, saturation line.

Table 5. Coefficients Used to Fit Eqs 9 and 10 (d_i, Density Units; c_j, Heat Capacity Units)

	d_i	c_j
i or j	kg m^{-3}	J kg^{-1} K^{-1}
0	2.003759E+03	−7.391193E+03
1	−3.776024E−01	7.801301E+01
2	−4.971029E−03	−2.417755E−01
3		2.548733E−04

This way, given an isobar of the density and of C_p, it is possible to integrate eqs 6 and 8 over the pressure (Sun et al., 1988) thus obtaining the (p,ρ,T) and (p,C_p,T) surfaces within the range of pressure and temperature of the experimental speed of sound data. The numerical integration procedure also allows the calculation of other properties, such as the isentropic compressibility, κ_S, the isothermal compressibility, κ_T, the ratio of the isobaric and isochoric heat capacities, γ, the isochoric heat capacity, C_v, the thermal pressure coefficient, γ_v, the isenthalpic Joule−Thomson coefficient, μ_{JT}, and the enthalpy and entropy variations relative to a reference state, ΔH and ΔS.

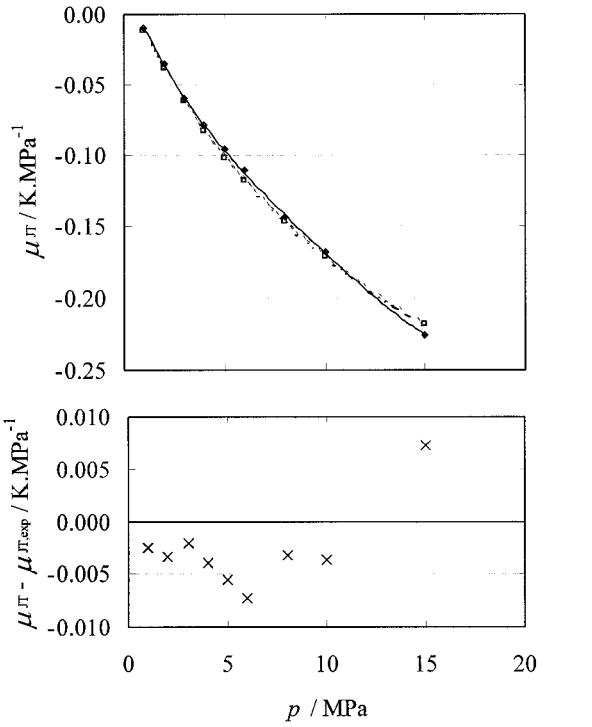

Figure 6. Plot of the calculated Joule−Thomson coefficient, μ_{JT}, isotherm at 303.15 K, and the deviations between those values and the data available in the literature, $\mu_{JT,exp}$ (Wirbser et al., 1992). Solid and dashed lines represent polynomial fits of each data set: ◆, literature; □, calculated; ×, deviation.

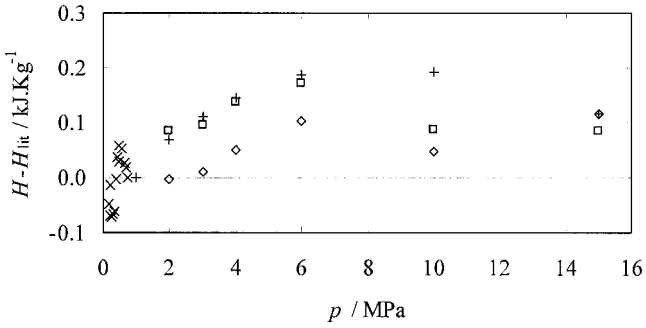

Figure 7. Deviations between the calculated enthalpy, H, and the data available in the literature, $H_{lit.}$ (Solvay leaflet on HFC227ea): ◇, 273.15 K; □, 288.15 K; +, 303.15 K; ×, saturation.

In the present work, the available experimental density (Klomfar et al., 1994) and isobaric heat capacity data (Wirbser et al., 1992) were interpolated to estimate an isobar of each of the two properties, at 10 MPa and from 270 K to 315 K. These isobars were fitted to eqs 9 and 10 with the coefficients of Table 5:

$$\rho(T,10\ \text{MPa}) = \sum_{i=0}^{2} d_i T^i \qquad (9)$$

$$C_p(T,10\ \text{MPa}) = \sum_{j=0}^{3} c_j T^j \qquad (10)$$

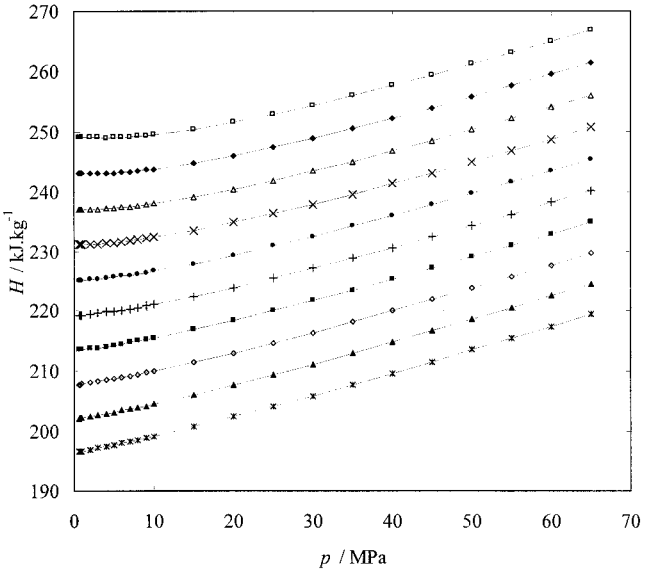

Figure 8. (p,H,T) surface, as a function of pressure: −∗−, 270 K; −▲−, 275 K; −◇−, 280 K; −■−, 285 K; −+−, 290 K; −●−, 295 K; −×−, 300 K; −△−, 305 K; −◆−, 310 K; −□−, 315 K.

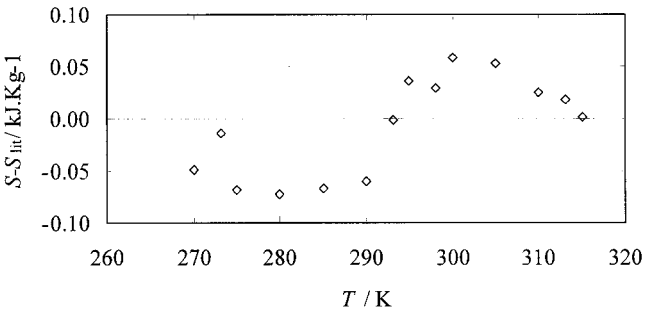

Figure 9. Plot of the deviations between the calculated entropy, S, and data from literature, S_{lit} (Solvay leaflet on HFC227ea), at saturation.

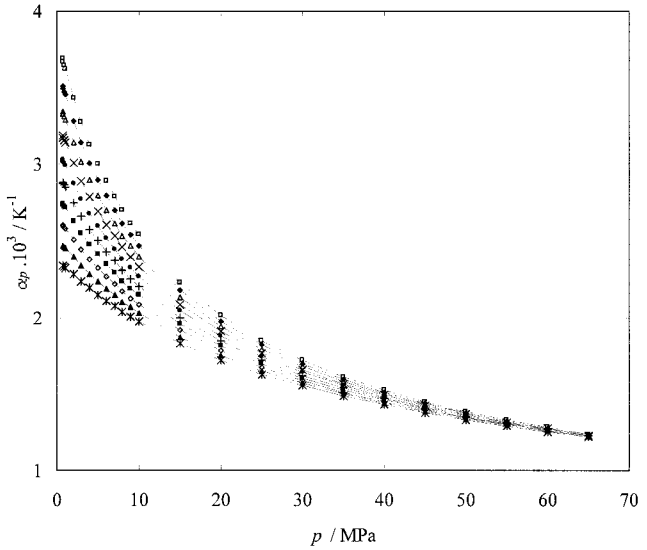

Figure 10. Thermal expansion coefficient data: −∗−, 270 K; −▲−, 275 K; −◇−, 280 K; −■−, 285 K; −+−, 290 K; −●−, 295 K; −×−, 300 K; −△−, 305 K; −◆−, 310 K; −□−, 315 K.

The integration procedure was implemented both on increasing pressure, up to 65 MPa, and on decreasing pressure, down to the saturation line. To test the results, the whole set of available experimental density data was fitted with an equation similar to eq 3, with a standard

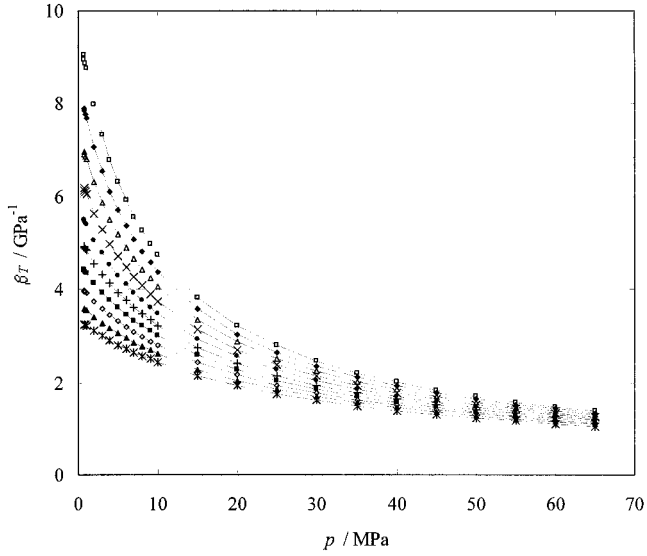

Figure 11. Isothermal compressibility data: −∗−, 270 K; −▲−, 275 K; −◇−, 280 K; −■−, 285 K; −+−, 290 K; −●−, 295 K; −×−, 300 K; −△−, 305 K; −◆−, 310 K; −□−, 315 K.

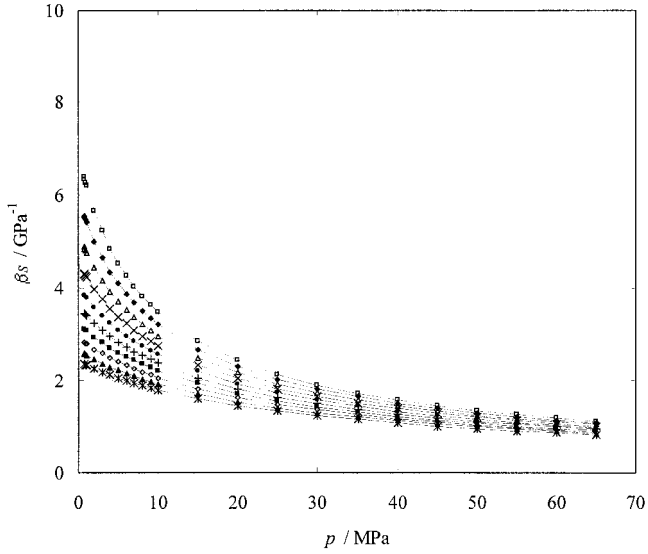

Figure 12. Isentropic compressibility data: −∗−, 270 K; −▲−, 275 K; −◇−, 280 K; −■−, 285 K; −+−, 290 K; −●−, 295 K; −×−, 300 K; −△−, 305 K; −◆−, 310 K; −□−, 315 K.

deviation that is better than ±0.04% in the low-pressure region and ±0.008% in the high-pressure region. Figure 3 represents the percent deviation between the integration results and the experimental densities (Klomfar et al., 1994). In the high-pressure region the integration results are in very good agreement with the experimental data, almost down to the magnitude of the accuracy of the experimental methods available for high pressures. In the lower pressure range, the deviations increase systematically with decreasing pressure, which is not unusual, since it is the region where the speed of sound measurements are more inaccurate. The second test of the method of calculation is the comparison of the calculated and experimental isobaric heat capacities (Wirbser et al., 1992). Figure 4 shows the percent deviations between the two data sets. The maximum deviation is smaller than ±0.75%, which points the uncertainty of the integration of the heat capacity to less than one percent, i.e., only one degree of magnitude above the density estimate, and certainly below the accuracy of the estimation methods based only upon equations of state. The complete (p,C_p,T) surface is plotted

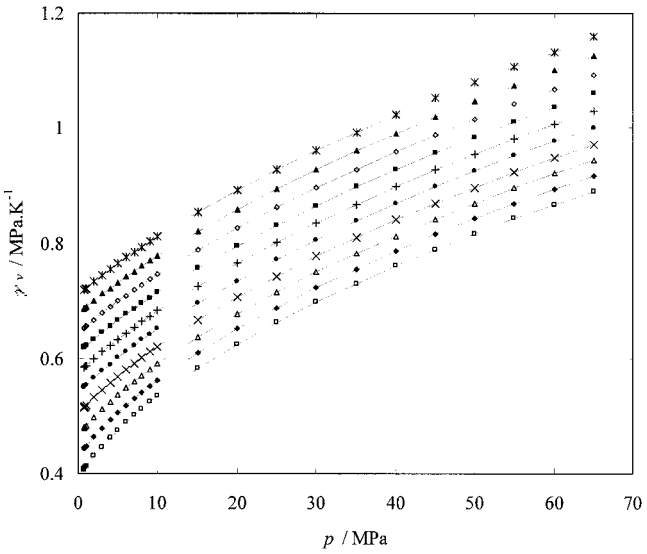

Figure 13. Thermal pressure coefficient data: −∗−, 270 K; −▲−, 275 K; −◇−, 280 K; −■−, 285 K; −+−, 290 K; −●−, 295 K; −×−, 300 K; −△−, 305 K; −◆−, 310 K; −□−, 315 K.

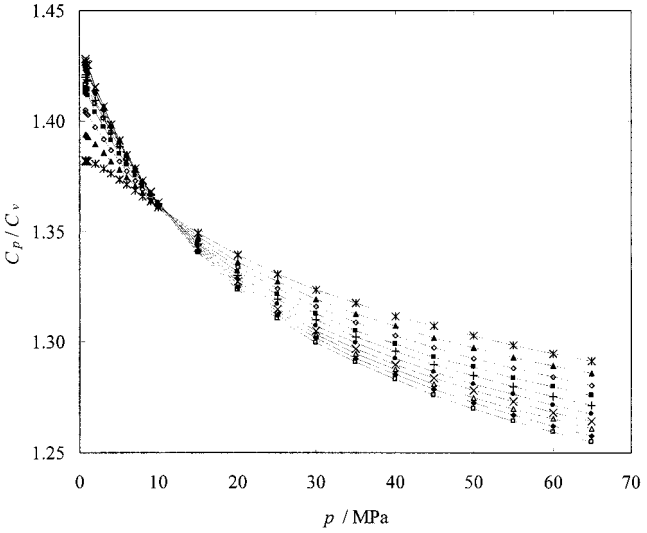

Figure 14. Ratio of isobaric and isochoric heat capacities: −∗−, 270 K; −▲−, 275 K; −◇−, 280 K; −■−, 285 K; −+−, 290 K; −●−, 295 K; −×−, 300 K; −△−, 305 K; −◆−, 310 K; −□−, 315 K.

in Figure 5. The experimental data available, overlapping the pressure and temperature range covered by our calculations, includes an isotherm of the Joule−Thomson coefficient μ_{JT}. Our values are compared to that isotherm (Wirbser et al., 1992) in Figure 6. Finally, we compare the variations of enthalpy and entropy with the data available (Solvay leaflet on HFC227ea). The reference state is the saturated liquid at the temperature of 273.15 K, with the arbitrary values of 200 kJ kg^{-1} for the enthalpy and 1 kJ kg^{-1} K^{-1} for the entropy. The deviations between our calculated enthalpies and literature values are plotted in Figure 7, in which the maximum deviation represents less than ±0.5% of the enthalpy variation (see Figure 8). The only entropy data found in the literature was the orthobaric, which is compared with our results in Figure 9.

The other thermodynamic properties calculated are represented in Figures 10−15.

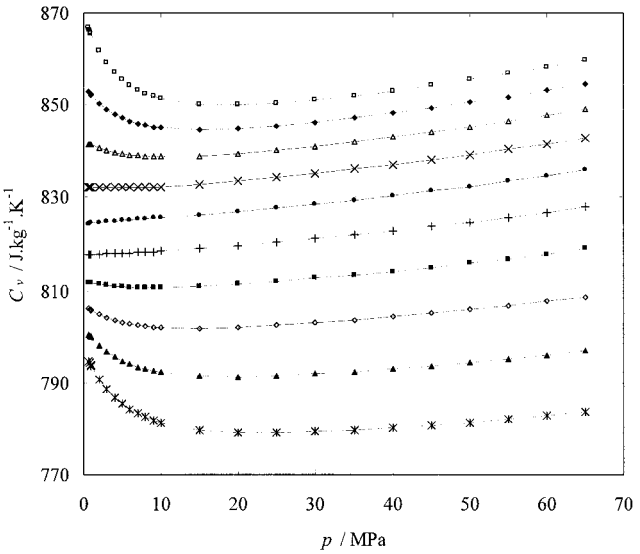

Figure 15. Isochoric heat capacity: −∗−, 270 K; −▲−, 275 K; −◇−, 280 K; −■−, 285 K; −+−, 290 K; −●−, 295 K; −×−, 300 K; −△−, 305 K; −◆−, 310 K; −□−, 315 K.

Summary

We have measured the speed of sound of HFC227ea with great accuracy. The experimental data were used to estimate, by a standard thermodynamic calculation method, several thermophysical properties. The estimated data were compared with the available literature data. The accuracy of the calculated values was found to be near, or even below, the average uncertainties of the usual experimental methods available.

Acknowledgment

The authors are grateful to Solvay Fluor und Derivate GmbH for providing the refrigerant sample.

Literature Cited

Klomfar, J.; Hrubý, J.; Sifner, O. *J. Chem. Thermodynamics* **1994**, *26*, 965−970.

Kyohara, O.; Alpin, C. J.; Benson, G. C. *J. Chem. Thermodyn.* **1978**, *10*, 721−730.

Lainez, A.; Miller, J. F.; Zollweg, J. A.; Streett, W. B. *J. Chem. Thermodyn.* **1987**, *19*, 1251−1260.

Pires, P. F.; Guedes, H. J. R. *J. Chem. Thermodyn.* **1999a**, *31*, 55−69.

Pires, P. F.; Guedes, H. J. R. *J. Chem. Thermodyn.* **1999b**, *31*, 479−490.

Sun, T.; Biswas, S. N.; Trappeniers, N. J.; Seldam, C. A. T. *J. Chem. Eng. Data* **1988**, *33*, 395−398.

Tuerk, M.; Zhai, J.; Nagel, M.; Bier, K. *Waermetechnik/Kaeltetechnik* **1994**, *79* (19), 1−71.

Weber, L. A.; Defibaugh, D. E. *J. Chem. Eng. Data* **1996**, *41*, 761−764.

White, G. K.; Roberts, R. B. *High Temp.−High Pressures* **1980**, *12*, 311−317.

Metals Handbook, 9th ed.; ASM: Strongsville, OH, 1979.

Wirbser, H.; Braeuning, G.; Guertner, J.; Ernest, G. *J. Chem. Thermodynamics* **1992**, *24*, 761−772.

Received for review November 2, 1999. Accepted February 15, 2000. The authors wish to thank the Fundação para a Ciência e Tecnologia for the financial support (grants BD/2522/93/RM and BTI/16572/98).

JE9902950